

Effect of Stresses and Strains of Roadway Surrounding Rocks on Borehole Airtightness**WU Wei^{1,2*}, WANG Zhaofeng^{1,2} and JEN An**¹Engineering Center of the Ministry of Education of Coal Mine Disaster Prevention and Disaster Relief, Henan Polytechnic University, Jiaozuo 454000, China²College of Safety Science and Engineering, Henan Polytechnic University, Jiaozuo 454000, China³RMIT University, Melbourne, Australia

Received 28 January 2016; Accepted 10 February 2016

Abstract

At present, many high gas and outburst mines have poor gas drainage effects. An important reason influencing the gas drainage effect is a poor hole-sealing effect. Most studies on gas drainage borehole sealing focus on local and foreign borehole sealing methods, borehole sealing equipment, and borehole sealing materials. Numerical simulations of initial drilling sealing depth are insufficient because studies on this subject are few. However, when the initial sealing depth of the borehole is not chosen reasonably, air can enter the gas drainage drill hole through the circumferential crack of roadway surrounding rocks under the influence of suction pressure of the drainage system. This phenomenon ultimately affects the hole-sealing effect. To improve the drilling hole sealing of gas drainage boring, we deduced the expression formulas of the crushing zone, plastic zone, and elastic zone around the coal-seam floor stone drift and conducted a stress-strain analysis of the coal-seam floor stone drift of the 2145 working surfaces of the Sixth Coal Mine of Hebi Coal Mine Group Company by using theoretical analysis, numerical simulation, and on-scene verification. Finally, we obtain the initial drilling sealing depth, which is a main contribution of this study. The results prove the following. The performed hole-sealing process with an initial drilling sealing depth of 8 m has a gas drainage efficiency of 55%. Compared with the previous 6.8 m initial drilling sealing depth with a gas drainage efficiency of less than 30%, which was adopted by the mine, the initial sealing depth of 8 m chosen in the numerical simulation is reasonable and conforms to the actual situation on the spot. Therefore, the initial drilling sealing depth chosen in the numerical simulation will produce practical and effective guidance to study the field hole-sealing depth.

Keywords: Gas Drainage, Hole Sealing, Numerical Simulation, Initial Drilling Sealing Depth

1. Introduction

Coal is one of the main energy resources in our country. Along with increasing mining depth, the probability of gas accidents also increases. In the 1950s, our country treated gas drainages as an important measure to prevent and control coal mine gas. After decades of development, gas drainage technology has made significant progress. At present, the main hole sealing ways in the country and abroad include mechanical cement mortar hole sealing [1,2], chemical grouting materials hole sealing [3,4], and hole sealing with hole packer. However, many gas and outburst mines still have a poor gas drainage effect in our country and the gas drainage rate cannot meet the standards. These deficiencies can be attributed to the poor gas permeability [5] of coal seams, improper choice of the gas drainage method, and poor effect of the borehole seal of gas drainage. If the initial sealing depth of gas drainage boring is not chosen reasonably, the hole-sealing effect will be directly influenced. The so-called initial drilling sealing depth denotes the distance from the orifice of the roadway drill hole inward up to the location where the adoption of the hole-sealing device begins. At present, studies on gas drainage borehole sealing focus on local and foreign borehole sealing methods, borehole sealing equipment, and

borehole sealing materials. Numerical simulations are insufficient because studies on initial drilling sealing depth are few. Hence, this study investigates the initial drilling sealing depth of gas drainage by conducting theoretical analyses, numerical simulations, and on-scene verifications. This study obtains an initial drilling sealing depth that is reasonable and matches with the actual situation; this result is one of the main contributions of this article. The following factors mainly cause the occurrence of the unreasonable choice of the initial sealing depth of gas drainage drill hole. The previous choice of the drill-hole initial sealing depth largely depends on the factors of on-site experience and geological conditions to judge the initial sealing location of the drill hole; this research includes theoretical analysis and numerical simulation, particularly the characteristics of the roadway surrounding stress-strain. Without investigation, the roadway surrounding stress-strain cannot be accurately judged only by on-site experience. Furthermore, the chosen initial sealing depth cannot evade the fissure of the roadway surrounding rock. Thus, the air leakage channel cannot be fixed when the drill hole is sealed. Under the influence of suction pressure of the drainage system, the air in the roadway can enter the tube used for gas drainage, thereby leading to the poor gas drainage effect through the fissure of roadway surrounding rocks [6–11]. Therefore, this work studies the effect of the stress-strain of roadway surrounding rocks on borehole seal depth by analyzing the stress-strain of roadway surrounding rocks. This work also finds reasonable hole-sealing positions and improves the whole

* E-mail address: hpuwuwei@163.com

sealing effect to achieve the aim of improving the gas drainage rate.

2. Stress-strain Relation of Roadway Surrounding Rock

For rock mass, the Mohr-Coulomb strength criterion is usually adopted. The shear strength τ of the rock mass depends on positive stress σ on the slip plane and the shear strength t is expressed as the function [12] of positive stress σ , i.e.,

$$\tau = f(\sigma) \tag{1}$$

If the envelope line is a straight line, the following is obtained (Fig. 1):

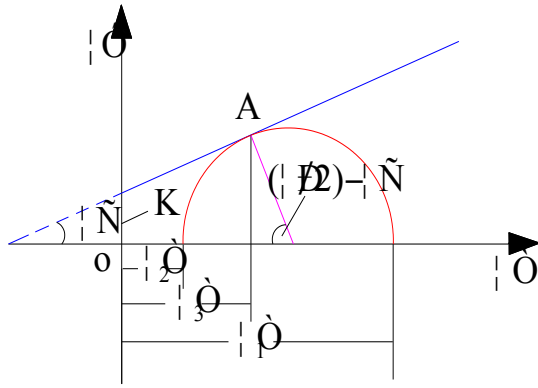


Fig. 1. Envelop of Mohr's circles of principal stresses

$$\tau = \sigma \tan \rho + K \tag{2}$$

Because

$$\begin{aligned} \tau &= \frac{\sigma_1 - \sigma_2}{2} \sin\left(\frac{\pi}{2} - \rho\right) = \frac{\sigma_1 - \sigma_2}{2} \cos \rho \\ \sigma &= \frac{\sigma_1 + \sigma_2}{2} - \frac{\sigma_1 - \sigma_2}{2} \cos\left(\frac{\pi}{2} - \rho\right) \\ &= \frac{\sigma_1 + \sigma_2}{2} - \frac{\sigma_1 - \sigma_2}{2} \sin \rho \end{aligned} \tag{3}$$

Hence,

$$\sigma_1 - \frac{1 + \sin \rho}{1 - \sin \rho} \sigma_3 = \frac{2 \cot \rho}{1 - \sin \rho} K \tag{4}$$

If σ_{com} is represented as the compressive strength of rock, when the elastic stage is reached. Formula (4) is then transformed as follows:

$$\sigma_1 - A\sigma_3 = \sigma_{com} \tag{5}$$

Thus, the shift to the stress-strain relation is represented by principal stress, as shown in Fig.2. The following formula is for the descending branch:

$$\sigma_1 - A\sigma_3 = \sigma_{com} - M\varepsilon_1' \tag{6}$$

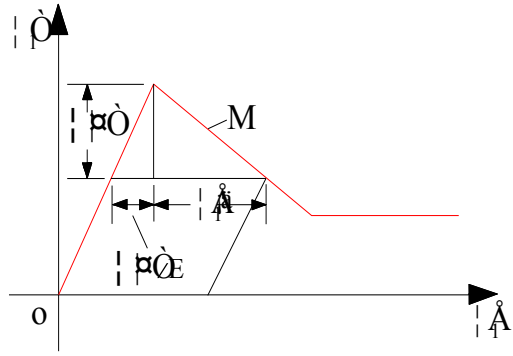


Fig. 2. Stress-strain relation curve with descending branch

In Formula (6), M is the modulus of the descending branch and is the deformation of the elastic region.

The following is obtained if the lateral deformation coefficient is introduced:

$$\beta = |\varepsilon_3' / \varepsilon_1'| \tag{7}$$

Thereafter, Formula (6) is transformed into the following:

$$\sigma_1 - A\sigma_3 = \sigma_{com} + M\varepsilon_3' / \beta \tag{8}$$

Suppose $\xi = M/E$. The following irreversible deformations are obtained:

$$\begin{aligned} \varepsilon_1^n &= \varepsilon_1' + \frac{\Delta\sigma}{E} = \varepsilon_1' + \frac{M\varepsilon_1'}{E} = \varepsilon_1'(1 + \xi) \\ &= \frac{(1 + \xi)}{M} (-\sigma_1 + A\sigma_3 + \sigma_{com}) \end{aligned} \tag{9}$$

and

$$\begin{aligned} \varepsilon_3^n &= \varepsilon_3' + \frac{\Delta\sigma}{E} = \beta\varepsilon_1' + \frac{M\varepsilon_1'}{E} = \varepsilon_1'(\beta + \xi) \\ &= \frac{(\beta + \xi)}{M} (\sigma_1 - A\sigma_3 - \sigma_{com}) \end{aligned} \tag{10}$$

For elastic deformation, the Poisson's ratio is $\nu = 0.5$; Thereafter,

$$\varepsilon_1^e = \frac{3}{4E} (\sigma_1 - \sigma_3), \varepsilon_3^e = -\varepsilon_1^e \tag{11}$$

The total deformation is expressed as follows:

$$\left. \begin{aligned} \varepsilon_1 &= \varepsilon_1^e + \varepsilon_1^n, \varepsilon_3 = \varepsilon_3^e + \varepsilon_3^n \\ M\varepsilon_1 &= a_1\sigma_1 + b_1\sigma_3 + c_1 \\ M\varepsilon_3 &= a_2\sigma_1 + b_2\sigma_3 + c_2 \end{aligned} \right\} \tag{12}$$

where

$$\begin{cases} a_1 = -(1 + 0.25\xi), a_2 = \beta + 0.25\xi \\ b_1 = A + \xi(A - 0.75), b_2 = -A\beta - \xi(A - 0.75) \\ c_1 = \sigma_{com}(1 + \xi), c_2 = -\sigma_{com}(\beta + \xi) \end{cases}$$

3. Stress-strain of Roadway Surrounding Rock Theory

Ground stress causes the formation of elasto-plastic range in the roadway surrounding rock [12, 13]. The elasto-plastic range of the roadway mainly includes the elastic region, plastic zone, and crushing zone. In the original rock stress far away from the roadway, the hoop strain $\varepsilon_\theta = 0$, approximating the stress condition with equal component of stress, i.e., $\sigma_\theta = \sigma_r$, whereas the original rock stress near the roadway is $\varepsilon_\theta > 0, \sigma_\theta > \sigma_r$; the stress condition can be met in the boundary r_{12} between the elastic region and initial stress area:

$$\sigma_\theta = A\sigma_r + \sigma_c \quad (13)$$

On the stress level, the strength of the rock mass σ_c is determined by the snap-in force, cohesive force, and friction force of the rock. After entering the elastic region, with increasing deformation ε_θ and the bevelment of the unevenness on the slip plane, the snap-in force gradually decreases. Hence, the hardness of the rock diminishes until the residual strength σ_0 is reached on boundary r_{23} between elastic region and plastic zone. The value of residual strength σ_0 is determined by the cohesive force and friction force of the rock mass. The stress condition is met on the following boundary:

$$\sigma_\theta = A\sigma_r + \sigma_0 \quad (14)$$

The deformation ε_θ cannot be unrestrictedly increased, and y is in the plastic zone. When the limit value ε_{cr} is reached, the inner cohesive force is changed to zero, i.e., $\sigma_0 = 0$; the rock mass will completely enter the collapse behavior, i.e., the boundary of the crushing zone. The plastic and crushing zone is r_{34} . The condition is met in the crushing zone, i.e.,

$$\sigma_\theta = A\sigma_r \quad (15)$$

The area influencing the borehole seal effect is mainly elasto-plastic range. The stress, strain, and size of the displacement in the area are theoretically analyzed as follows.

In the elastic zone, assume that the constitutive relationship is described by the following equation:

$$\sigma_\theta - A\sigma_r = \sigma_c - M\varepsilon'_\theta, \varepsilon'_r = -\beta_0\varepsilon'_\theta \quad (16)$$

The total deformation should be written as follows:

$$\varepsilon_\theta = \frac{3}{2E} \frac{(A-1)q + \sigma_c}{A+1} + \varepsilon'_\theta \quad (17)$$

and

$$\varepsilon_r = -\frac{3}{2E} \frac{(A-1)q + \sigma_c}{A+1} - \beta_0\varepsilon'_\theta \quad (18)$$

The following equation is solved by considering Formulas (17) and (18):

$$\frac{d\varepsilon_\theta}{dr} + \frac{\varepsilon_\theta - \varepsilon_r}{r} = 0 \quad (19)$$

The following strain representation in the elastic zone is obtained on the basis of boundary conditions $r = r_{12}$ and $\varepsilon'_\theta = 0$:

$$\varepsilon'_\theta = \frac{3}{E} \frac{(A-1)q + \sigma_c}{(A-1)(1+\beta_0)} \left[\left(\frac{r_{12}}{r} \right)^{1+\beta_0} - 1 \right] \quad (20)$$

We substitute Formula (20) into Formula (16) and represent the stress component with stress function $F(r)$:

$$\sigma_r = \frac{F}{r}, \sigma_\theta = \frac{dF}{dr} \quad (21)$$

We obtain

$$\frac{dF}{dr} - A\frac{F}{r} = \sigma_c - 3\xi \frac{(A+1)q + \sigma_c}{(A+1)(1+\beta_0)} \left[\left(\frac{r_{12}}{r} \right)^{1+\beta_0} - 1 \right] \quad (22)$$

In Formula (22), $\xi = M/E$.

We solve Formula (22) by considering $\sigma_r = \sigma_{23}$ on boundary $r = r_{23}$ and placing the solution as follows:

$$\left. \begin{aligned} \sigma_r &= \frac{[(A+1)(1+\beta_0) + 3\xi]\sigma_c + 3\xi(A-1)q}{(A^2-1)(1+\beta_0)} \\ &\left[\left(\frac{r}{r_{23}} \right)^{A-1} - 1 \right] + 3\xi \frac{(A-1)q + \sigma_c}{(A+1)(1+\beta_0)(A+\beta_0)} \\ &\left[\left(\frac{r_{12}}{r} \right)^{1+\beta_0} - \left(\frac{r_{12}}{r_{23}} \right)^{1+\beta_0} \left(\frac{r}{r_{23}} \right)^{A-1} \right] + \sigma_{r3} \left(\frac{r}{r_{23}} \right)^{A-1} \\ \sigma_\theta &= A\sigma_r + \sigma_c - 3\xi \frac{(A-1)q + \sigma_c}{(A+1)(1+\beta_0)} \left[\left(\frac{r_{12}}{r} \right)^{1+\beta_0} - 1 \right] \\ \tau_{r\theta} &= 0 \end{aligned} \right\} \quad (23)$$

In Formula (23), σ_{r3} is the stress on the boundary r_{23} . We obtain from the stress analysis of the plastic zone as follows.

The deformed component in the plastic zone is determined in the following formula from (17) to (20):

$$\left. \begin{aligned} \varepsilon_\theta &= \frac{3}{2E} \frac{(A-1)q + \sigma_c}{A+1} \left\{ 1 + \frac{2}{1+\beta_0} \left[\left(\frac{r_{12}}{r} \right)^{1+\beta_0} - 1 \right] \right\} \\ \varepsilon_r &= -\frac{3}{2E} \frac{(A-1)q + \sigma_c}{A+1} \left\{ 1 + \frac{2\beta_0}{1+\beta_0} \left[\left(\frac{r_{12}}{r} \right)^{1+\beta_0} - 1 \right] \right\} \end{aligned} \right\} \quad (24)$$

Thus, by resorting to geometric equations $\varepsilon_r = du/dr$ and $\varepsilon_\theta = u/r$, we can obtain the radial displacement as follows:

$$u = r \frac{3}{2E} \frac{(A-1)q + \sigma_c}{A+1} \left\{ 1 + \frac{2}{1+\beta_0} \left[\left(\frac{r_{12}}{r} \right)^{1+\beta_0} - 1 \right] \right\} \quad (25)$$

If the irreversible deformation on boundary r_{23} is $\varepsilon'_\theta = (\sigma_c - \sigma_0)/M$, the relation between r_{12} and r_{23} from Formula (20) is expressed as follows:

$$\frac{r_{12}}{r_{23}} = \left[1 + \frac{(\sigma_c - \sigma_0)(A+1)(1+\beta_0)}{3\xi(A-1)q + 3\xi\sigma_c} \right]^{\frac{1}{1+\beta_0}} \quad (26)$$

In the plastic zone, the governing equation is a balance equation and physical equation:

$$\frac{d\sigma_r}{dr} + \frac{\sigma_r - \sigma_\theta}{r} = 0, \sigma_\theta = A\sigma_r + \sigma_0 \quad (27)$$

On the basis of the above-mentioned equation, with respect to the stress σ_{r4} on the boundary with crushing zone r_{34} , the stress representation of the plastic zone is as follows:

$$\left. \begin{aligned} \sigma_r &= \left(\frac{\sigma_0}{A-1} + \sigma_{r4} \right) \left(\frac{r}{r_{34}} \right)^{A-1} - \frac{\sigma_0}{A-1} \\ \sigma_\theta &= A \left(\frac{\sigma_0}{A-1} + \sigma_{r4} \right) \left(\frac{r}{r_{34}} \right)^{A-1} - \frac{\sigma_0}{A-1}, \tau_{r\theta} = 0 \end{aligned} \right\} \quad (28)$$

The deformed component in this area is obtained by the deformation continuity equation $d\varepsilon_\theta/dr + (\varepsilon_\theta - \varepsilon_0)/r = 0$, incompressible condition $\Delta\varepsilon'_1 + \Delta\varepsilon'_3 = 0$, and deformation boundary condition on boundary r_{23} :

$$\left. \begin{aligned} \varepsilon_\theta &= \frac{(1-\beta_0)(\sigma_c - \sigma_0)}{2M} + \frac{3}{2E} \frac{(A-1)q + \sigma_c}{A+1} \left(\frac{r_{12}}{r_{23}} \right)^{1+\beta_0} \left(\frac{r_{23}}{r} \right)^2 \\ \varepsilon_r &= \frac{(1-\beta_0)(\sigma_c - \sigma_0)}{2M} - \frac{3}{2E} \frac{(A-1)q + \sigma_c}{A+1} \left(\frac{r_{12}}{r_{23}} \right)^{1+\beta_0} \left(\frac{r_{23}}{r} \right)^2 \end{aligned} \right\} \quad (29)$$

The radial dispersion is obtained by $\varepsilon_\theta = u/r$:

$$u = \frac{(1-\beta_0)(\sigma_c - \sigma_0)}{2M} r + \frac{3}{2E} \frac{(A-1)q + \sigma_c}{A+1} \left(\frac{r_{12}}{r_{23}} \right)^{1+\beta_0} \frac{r_{23}^2}{r} \quad (30)$$

On boundary r_{34} between the plastic zone and crushing zone, the radial displacement or circumferential deformation ε_θ reaches a certain limit; the cohesive force is zero in the rock mass. From Formula (29), where $\varepsilon_\theta = \varepsilon_{cr}$ and $r = r_{34}$, the following relation between r_{23} and r_{34} can be obtained as follows:

$$\frac{d\sigma_r}{dr} + \frac{\sigma_r - \sigma_\theta}{r} = 0, \sigma_\theta = A\sigma_r. \quad (31)$$

In the crushing zone, the governing equation is a balance equation and physical equation:

$$\frac{r_{23}}{r_{34}} = \left\{ \frac{(A+1)[2M\varepsilon_{cr} + (\beta_0 - 1)(\sigma_c - \sigma_0)]}{3\xi(A-1)q + 3\xi\sigma_c + (A+1)(\beta_0 + 1)(\sigma_c - \sigma_0)} \right\}^{\frac{1}{2}} \quad (32)$$

On the roadway border when the boundary condition $r = 1$ is satisfied, $\sigma_\theta = p$, i.e.,

$$\sigma_r = pr^{A-1}, \sigma_\theta = Apr^{A-1}, \tau_{r\theta} = 0 \quad (33)$$

The deformed component by $d\varepsilon_\theta/dr + (\varepsilon_\theta - \varepsilon_0)/r = 0$, incompressibility condition $\Delta\varepsilon'_1 + \Delta\varepsilon'_3 = 0$, and $\varepsilon_\theta = \varepsilon_{cr}$ on $r = r_{34}$ obtains the following:

$$\left. \begin{aligned} \varepsilon_\theta &= \frac{(1-\beta_0)(\sigma_c - \sigma_0)}{2M} + \left[\varepsilon_{cr} - \frac{(1-\beta_0)(\sigma_c - \sigma_0)}{2M} \right] \left(\frac{r_{34}}{r} \right)^2 \\ \varepsilon_r &= \frac{(1-\beta_0)(\sigma_c - \sigma_0)}{2M} - \left[\varepsilon_{cr} - \frac{(1-\beta_0)(\sigma_c - \sigma_0)}{2M} \right] \left(\frac{r_{34}}{r} \right) \end{aligned} \right\} \quad (34)$$

The corresponding radial displacement is expressed as follows:

$$\varepsilon_\theta = r \frac{(1-\beta_0)(\sigma_c - \sigma_0)}{2M} + r \left[\varepsilon_{cr} - \frac{(1-\beta_0)(\sigma_c - \sigma_0)}{2M} \right] \left(\frac{r_{34}}{r} \right) \quad (35)$$

The stress on the boundary $r = r_{34}$ is expressed as follows:

$$\sigma_r = pr_{34}^{A-1} \quad (36)$$

Thus, the following is obtained from Formulas (28) and (35), where $r = r_{23}$:

$$\sigma_{r3} = \left(\frac{\sigma_0}{A-1} + pr_{34}^{A-1} \right) \left(\frac{r_{23}}{r_{34}} \right)^{A-1} - \frac{\sigma_0}{A-1} \quad (37)$$

Thus, the stress-strain state in the elasto-plastic zone depends on its radius. Suppose Formulas (13) and (23) are equal when $r=r_{12}$, we obtain the following when considering Formula (37):

$$pr_{12}^{A-1} = q - \frac{(A-1)q + \sigma_c}{A+1} - \frac{\sigma_0}{A-1} \left(\frac{r_{12}}{r_{23}} \right)^{A-1} \left[\left(\frac{r_{23}}{r_{12}} \right)^{A-1} - 1 \right] - \frac{[(A+1)(1+\beta_0) + 3\xi]\sigma_c + 3\xi(A-1)q}{(A^2+1)(1+\beta_0)} \left[\left(\frac{r_{12}}{r_{23}} \right)^{A-1} - 1 \right] + \frac{3\xi(A-1)q + 3\xi\sigma_c}{(A+1)(1+\beta_0)(A+\beta_0)} \left[\left(\frac{r_{12}}{r_{23}} \right)^{A+\beta_0} - 1 \right] \quad (38)$$

After determining r_{12} , r_{23} and r_{34} can be completely determined by Formulas (26) and (31).

The ideal plasticity solution is obtained when the above-mentioned solutions is $\xi \rightarrow 0$, $\sigma_0 = \sigma_c$, and $r_{23} = r_{12} = 1$. The ideal brittleness of the rock mass can be obtained when $\xi \rightarrow 0$, $\sigma_0 = \sigma_c$, $r_{23} = r_{12}$, and $r_{34} = 1$. In both cases, the border radius in the elastic zone and original rock stress zone is expressed as follows.

For an ideal brittle material:

$$r_{12} = \left[\left(\frac{2q - \sigma_c}{A+1} + \frac{\sigma_0}{A-1} \right) \left(\frac{A-1}{Ap - p + \sigma_0} \right) \right]^{\frac{1}{A+1}} \quad (39)$$

For an ideal plastic material:

$$r_{12} = \left[\left(\frac{2q - \sigma_c}{A+1} + \frac{\sigma_0}{A-1} \right) \left(\frac{A-1}{Ap - p + \sigma_c} \right) \right]^{\frac{1}{A+1}} \quad (40)$$

In both cases, the radial displacement in the crushing zone is:

$$u = \frac{3}{2E} \frac{(A-1)q + \sigma_c}{A+1} \frac{r_{12}^2}{r} \quad (41)$$

In the crushing zone, the rock mass is in a state of destruction. We rely on frictional resistance to maintain stability. Frictional resistance is caused by tangential stress, which is around the roadway generated by the block. In the plastic zone, the rock mass is in the plastic stage of the compression deformation. Under the influence of stress redistribution, an internal crack produces a new certain direction of the fracture weak plane. Both the size of the area of the physical and mechanical properties of rock mass and original rock stress field distribution of the state have a close relationship. This relationship has been previously analyzed. In the elastic zone, the rock mass is at the stage of elastic deformation under the action of external force. The majority of the interior crack is located in the initial fissure weak plane, which is under the action of new stress [14, 15]. The spatial scale of the fracture weak plane has certain changes, but the rock mass is still in the stage of elastic deformation. According to the theoretical analysis, ground stress will

increase in the elastic zone and the rock mass will have certain permeability. In terms of distance away from the roadway, is the original rock stress zone is beyond the elastic region. The rock mass can be treated as an area that is unaffected by roadway formation. Thus, the roadway surrounding rock mass within the borehole seal must bypass the elasto-plastic range because the permeability and mechanical state of the rock mass will change in the elasto-plastic range of the roadway. More air leakage passages exist because the region fractures are greater in number. Borehole sealing should not be performed in this area, even if hole sealing is conducted in this area. The effect of this process is also poor.

4. Stress-strain of Roadway Surrounding Rock Numerical Simulation and Initial Sealing Depth

On the basis of the theoretical investigation of the elastic, plastic, and crushing zones of the roadway, we perform the numerical simulation research on the stress-strain of the seam-floor stone-drift surrounding rock by adopting COMSOL multiphysics numerical simulation software. On the basis of the result of the roadway surrounding rock stress-strain obtained from the simulation computation, the reasonable drill-hole initial sealing depth is finally chosen.

We used 2145 working surfaces of the coal-seam floor of the stone-drift crossing drill hole of Hebi Coal Mine Group Company's Sixth Coal Mine, e.g., performed the sample numerical simulation. According to the calculation results, the reasonable initial sealing depth is determined for the coal-seam floor of the drill hole of the stone-drift crossing. The cover depth of the 2145 working surfaces of the coal-seam floor stone drift of Hebi Coal Mine Group Company's Sixth Coal Mine is 500 m or so with a strike length of 980 m located in the sandstone rock stratum.

We perform the stress-strain numerical simulation of the roadway with a cover depth of 500 m and radius of 2.5 m by adopting the Mohr-Coulomb criterion. The roadway cover depth is 500 m; thus, the ground stress is 15 MPa. A ground stress of 15 MPa should be imposed on the upper, left, and right boundaries of the model established by choice(Fig.3 and Fig.4). The lower boundary is set as a fixed boundary. The physical mechanic property of the sandstone will be chosen as the physical parameter of the roadway surrounding rock mass (as shown in Table 1) because the roadway is arranged in the rock stratum of sandstone. AS shown in the table, Young's modulus is 2×10^4 MPa, the cohesive force is 19 MPa, internal friction angle is 39° , Poisson ratio is 0.2, and the density is 2.5 g/cm^3 . The balance equation adopting the elasticity of solid deformation is expressed as follows:

$$-\sigma_{ij,j} = F_i, (i, j = 1, 2, 3) \quad (42)$$

In Formula (42), σ_{ij} is the stress tensor and F_i is the volume force.

Table 1. Mechanical parameters of the model

Rock type	Young's modulus (MPa)	Cohesive force (MPa)	Internal friction Angle (unit $^\circ$)	Poisson ratio	Density (unit g/cm 3)
Sandstone	2×10^4	19	39	0.2	2.5

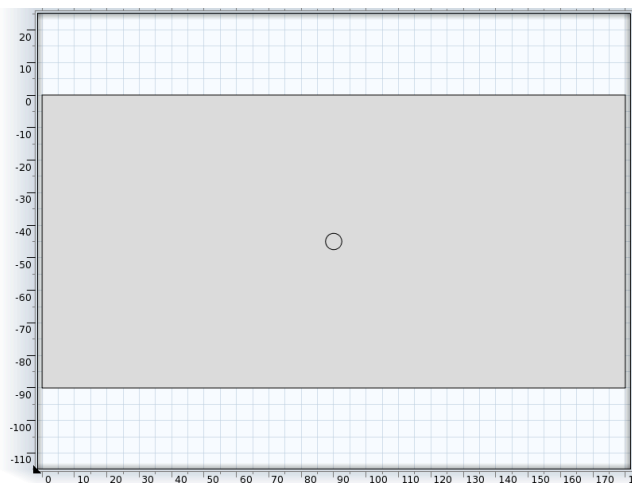


Fig. 3. Numerical simulation modeling diagram

The meshing model is shown in Fig. 4.

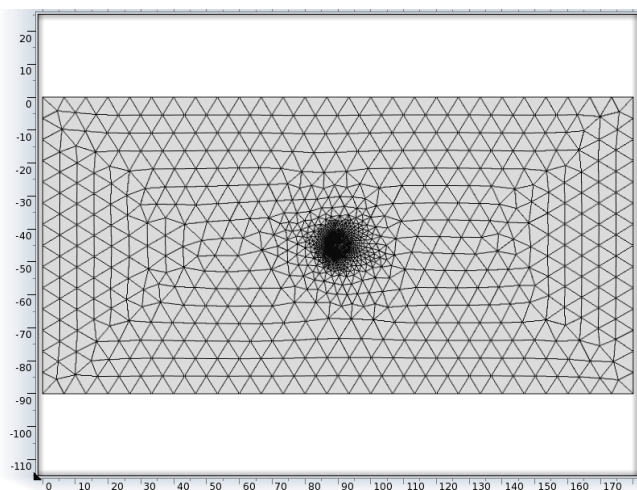


Fig. 4. Meshing figure diagram

Finally, we obtain the roadway surrounding rock stress diagram (Fig. 5) and the roadway surrounding rock strain diagram (Fig. 6).

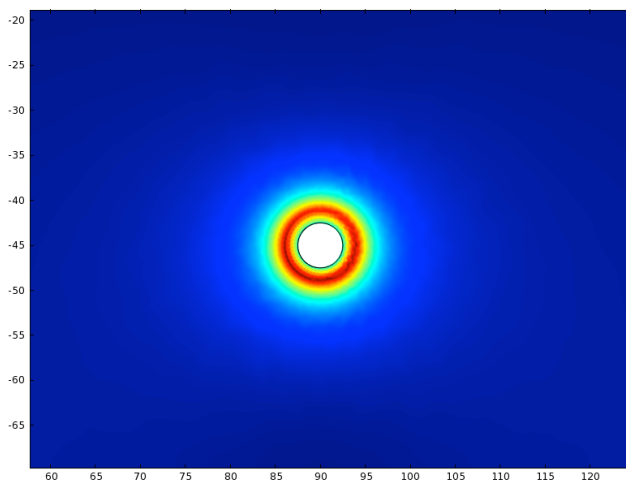


Fig. 5. Roadway surrounding rock stress diagram

In Fig.6, near the stone drift of the 2145 seam floor, particularly the area with the stone-drift center of circle as the reference frame, i.e., the rock mass in the green area

wherein the elastic-plastic behavior is shown, the elasto-plastic range is 10.5 m. The elasto-plastic range is 8 m from the roadway side wall where the rock mass deforms, and the gas permeability of surrounding rock is increased to a certain extent. The gas drainage borehole sealing in the coal-seam floor stone drift must avoid a mining-influenced area because the original rock excavated will destroy the original stress state of the roadway surrounding rock and lead to stress redistribution. On one hand, radial stress decreases the roadway perimeter to zero; on the other hand, the tangential stress increases, thus producing the stress concentration. Furthermore, the stress state of the surrounding rock becomes an approximately two-direction force. The previous state is a three-direction force, and stress conditions deteriorate. If the value of stress concentration is greater than the strength of the loose surrounding rock, a surrounding rock fracture will occur. This fracture from the roadway perimeter begins to gradually expand downward until a new three-direction force state of equilibrium is reached. At this point, the surrounding rock area will appear in a region. The region is called the elasto-plastic range, which is a process of occurrence, development, and stability. The value after the elasto-plastic range stabilizes reflects the surrounding rock stress and surrounding rock strength factors, such as the result of joint action.

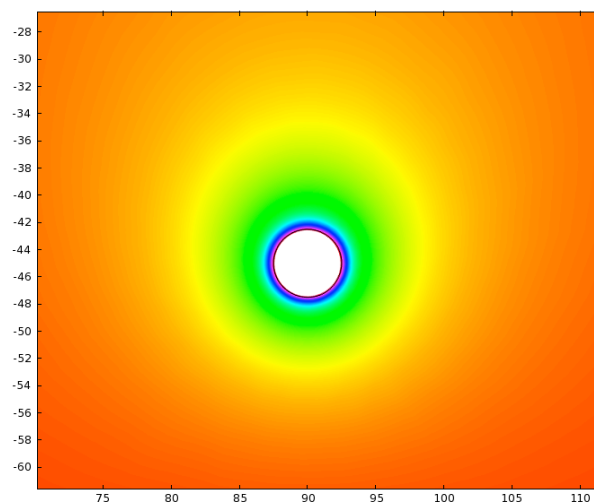


Fig. 6. Roadway surrounding rock strain diagram

A large number of field test results show the following. The destruction of roadway surrounding rock in coal-mine production is inevitable. Even in a low stress field, the surrounding rock of roadway under the effect of ground stress is also hard to stabilize. The mechanical characteristics of the roadway surrounding rock show that the stress-reducing area includes the crushing, plastic, and elastic zones. The loose rock mass mainly contains microcracks, which will increase gradually. Deformation suddenly increases, and cohesion and angle of internal friction are reduced. The loose rock mass fracture system develops, and a low stress value will have adverse effects on drill-hole sealing. On one hand, hole-sealing grout leaks outward along the elasto-plastic range of fracture system. On the other hand, the development of the fissure system is difficult to achieve full blocking for sealing. Thus, at the present stage, gas drainage borehole sealing must be conducted outside the roadway elasto-plastic range. In this region, fracture develops, air leakage passage increases. Under negative pressure gas drainage, outside air

can enter the cracks on the internal gas drainage pipe, which will seriously affect the gas drainage. If the area is chosen for the hole sealing, even if the hole sealing is completed, the effect can be poor under the suction pressure of the drainage system. Air leakage can result in this area. Thus, we avoid the area when selecting the initial sealing location, i.e., the boring initial sealing depth shall not be lower than 8 m.

A drilling field contains a seven-row gas drainage drill. Each row has five gas drainage drills. The total drilling is 35. The distance between one end of the drill hole and another is 5 m. We drilled using cement mortar hole sealing. The initial sealing depth of gas drainage drilling is 8 m. Each group of the five gas drainage drills is connected. We use one drainage pore plate to investigate the drainage concentration and flow orifice. In the end, the current collector was connected to the drainage pump station. In the 2145 working surface coal-seam floor stone drift on the site verify gas drainage efficiency. Compared with the previous case of on-site hole sealing, the initial sealing depth is less than 8 m. When the initial sealing depth of the on-site hole sealing is more than 8 m, gas drainage efficiency is from less than 30%–55%. The cumulative drainage gas data are 1.4 million m³. The hole is sealed closely. A single group of gas drainage concentration is more than 30%. Compared with the previous gas drainage concentration, the obtained drainage concentration is enhanced by nearly two times. Drainage negative pressure is 20 kpa, which has made significant drainage effect. Thus, the initial sealing depth of 8 m is reasonably and reliably chosen in the numerical simulation, which is in line with the actual situation.

5 Discussion

As a basic technical means for controlling gas, gas drainage drilling sealing has extensive application ranges in mine areas. In our country, however, the sealing quality of various drillings is unsatisfactory. Thus, research on initial drilling sealing depth should include the study of the stress–strain theory and numerical simulation of the seam-floor stone drift surrounding rock. To improve the utilization ratio of sealing, accelerate elimination outburst rate of coal seam, reduce the number of drilling, and save production cost, studies on initial drilling sealing depth have very important realistic significance in preventing serious accidents, such as gas outburst and gas explosion. At present, gas drainage borehole sealing studies focus more on borehole sealing

depth, borehole sealing equipment, and borehole sealing materials in the country and abroad because studies on initial drilling sealing depth are few, and numerical simulations are insufficient. Hence, this article studies gas drainage initial drilling sealing depth using theoretical analysis, numerical simulation, and on-scene verification. We have obtained initial drilling sealing depth that is reasonable and in line with the actual situation, which is also the innovation of this article.

The main results in this thesis are as follows: we analyzed the distribution of the stress field and strain field around the coal-seam floor stone drift, deduced the expression formulas of the crushing zone, plastic zone, and elastic zone around the coal-seam floor stone drift. Some conclusions are obtained from the theoretical analysis and numerical simulation. Sealing rock fracture is formed around the coal-seam floor stone drift. On the basis of the research on the stress–strain theory of the seam-floor stone drift surrounding rock, we simulate the stress–strain of the seam-floor stone drift surrounding rock by adopting the COMSOL multiphysics numerical simulation software. We combine the 2145 working surfaces of the coal-seam floor of stone-drift field cases of the Sixth Coal Mine of the Hebi Coal Mine Group Company according to the results of numerical simulation. A reasonable and reliable initial sealing depth of 8 m is chosen for the seam-floor stone-drift crossing drill hole, with reference to the actual hole-sealing depth of 8 m adopted in the field. The gas drainage efficiency is 55%, in contrast to the hole-sealing depth of 6.8 m, which was previously adopted by the mines. The gas drainage efficiency of less than 30% indicates that the research on hole-sealing depth with numerical simulation can accurately predict the elasto-plastic zone of the roadway. The same can be used as the basis of choice of the hole-sealing depth for the coal-mine seam-floor stone-drift crossing drill hole, which lays the foundation in enhancing the hole-sealing quality and effect, as well as gas drainage efficiency, boasting worthwhile advancement and application prospects.

Acknowledgements

This research was supported by the Specialized Research Foundation for the Doctoral Program of National Natural Science Foundation of China (No. 51274090 and 51374093) and Key Laboratory of Gas Geology and Gas Control of Henan Province, Provincial Department of Construction of State Key Laboratory Breeding Base Open Funded Projects (WS2012B01).

References

- Ogilvie, Michael L., Gas drainage in Australian underground coal mines”, *Mining Engineering: Littleton, Colorado*, 47(1), 1995, pp. 50-52.
- Hebble White B K, Richmond A J, Allan J., “Australian experience in long-hole in-seam drilling technology for seam gas drainage”, *Symposia Series-Australasian Institute of Mining and Metallurgy*, 33, 1982, pp.202-217.
- Noack, Klaus, “Control of gas emissions in underground coal mines”, *International Journal of Coal Geology*, 35(1/4), 1998, pp.57-82.
- Wanghua Sui, Jinyuan Liu, Wei Hu, et al, “Experimental investigation on sealing efficiency of chemical grouting in rock fracture with flowing water”, *Tunnelling and Underground Space Technology*, 50, 2015, pp.239-249.
- Chao Zhang, Baiquan Lin, Yan Zhou, et al, “Study on “fracturing-sealing” integration technology based on high-energy gas fracturing in single seam with high gas and low air permeability”, *International Journal of Mining Science and Technology*, 23(6), 2013, pp.841-846.
- Manchao He, “Physical modeling of an underground roadway excavation in geologically 45° inclined rock using infrared thermography”, *Engineering Geology*, 121, 2011, pp.165-176.
- Baiquan Lin, Fazhi Yan, Chuanjie Zhu, et al, “Cross-borehole hydraulic slotting technique for preventing and controlling coal and gas outbursts during coal roadway excavation”, *Journal of Natural Gas Science and Engineering*, 26, 2015, pp.518-525.
- Zhiyong Hao, Baiquan Lin, Yabin Gao, et al, “Establishment and application of drilling sealing model in the spherical grouting mode based on the loosening-circle theory”, *International Journal of Mining Science and Technology*, 22(6), 2012, pp.895-898.

9. Jianbing Peng, Liwei Chen, Qiangbing Huang, "Physical simulation of ground fissures triggered by underground fault activity", *Engineering Geology*, 155, 2013, pp. 19-30.
10. Yabin Gao, Baiquan Lin, Wei Yang, et al, "Drilling large diameter cross-measure boreholes to improve gas drainage in highly gassy soft coal seams", *Journal of Natural Gas Science and Engineering*, 26, 2015, pp.193-204.
11. Tingkan Lu, Zhaofeng Wang, Hongming Yang, et al, "Improvement of coal seam gas drainage by under-panel cross-strata stimulation using highly pressurized gas", *International Journal of Rock Mechanics and Mining Sciences*, 77, 2015, pp.300-312.
12. Chengzhi Qi, Qihu Qian, "Basic Problem of Dynamic Deformation and Fracture of Rock Mass", Science press, China, Beijing, 2009.
13. Wenxiu Li, Chongyang Gao, Xia Yin, et al, "A visco-elastic theoretical model for analysis of dynamic ground subsidence due to deep underground mining", *Applied Mathematical Modelling*, 39, 2015, pp.5495-5506.
14. Lan Cui, Junjie Zheng, Rongjun Zhang, et al, "Elasto-plastic analysis of a circular opening in rock mass with confining stress-dependent strain-softening behavior", *Tunneling and Underground Space Technology*, 50, 2015, pp.94-108.
15. Z.B. Liu, S.Y. Xie, J.F. Shao, et al, "Effects of deviatoric stress and structural anisotropy on compressive creep behavior of a clayey rock", *Applied Clay Science*, 114, 2015, pp.491-496.